Classifying Reactive Power Control Laws of Behind-the-Meter Solar Photovoltaic Inverters

Richard Asiamah*, Samuel Talkington*, Michael Boateng*, Marta Vanin†, Frederik Geth‡, Daniel K. Molzahn*
*Georgia Institute of Technology
{asiamah, talkington, mboateng6, molzahn}@gatech.edu
†KU Leuven
{marta.vanin}@kuleuven.be
‡GridQube
{frederik.geth}@gridqube.com

***Abstract*—Various types of reactive power control laws are heterogeneously used for inverter-based resources (IBRs) in distribution grids. As a result, grid operators may not be aware of *which type* of control law is used by a particular IBR. Different control laws imply different voltage support behaviors, which need to be known for the development of accurate computational models for power system analyses. To help mitigate this challenge, this paper develops two *classification* algorithms to identify which type of control law governs the reactive power output of a behind-the-meter solar photovoltaic inverter when the specific control law selected by the IBR owner is unknown. In particular, the two algorithms require only aggregated smart meter measurements to identify candidate reactive power control laws (constant power factor or volt-var control) for distribution network inverters. We present a case study to assess their classification accuracy and evaluate the algorithms' performance in the context of noisy measurements. Our neural network-based classifier is shown to have a higher classification accuracy and performs better under varying levels of noise.**

***Index Terms*—Reactive power control, inverters, classification, neural networks, distribution networks, system identification**

I. Introduction

Reactive power control of inverter-based assets is a crucial feature for advanced distribution management systems. Thus, there is significant research interest in the design [1], [2] and analysis [3], [4] of inverter control characteristics, as well as their stability assessment [5]. Historically, solar photovoltaic (PV) inverters were often operated in constant power factor mode (lagging to mitigate voltage rise). However, more recently, piece-wise linear volt-var control with a deadband has gained popularity, as it is superior at mitigating extreme voltage swings while avoiding unnecessary reactive flows at normal voltages. In practice, standards such as IEEE 1547-2018 [6] provide references for utilities to shape their interconnection requirements (see, e.g., the Hawaiian Rule 14H [7]). In Australia and New Zealand, the AS/NZS 4777.2 standard [8] specifies the requirements for inverters in low-voltage networks.

Support from NSF AI Institute for Advances in Optimization (AI4OPT) #2112533 and PSERC project T-67: Smart Meter-Driven Distribution Grid Visibility and Control. The work of S. Talkington is supported by the NSF Graduate Research Fellowship Program under Grant No. DGE-1650044. Any opinions, findings, and conclusions or recommendations expressed in this material are those of the author(s) and do not necessarily reflect the views of the National Science Foundation.

However, it is common for network operators to be unaware of the control laws selected for individual PV inverters; these are usually set by inverter control designers, installers, and field engineers and are not reported or logged by the distribution utility. The decentralized nature of these activities and responsibilities, in addition to the loss of system information, may ultimately lead to violations of grid connection standards (e.g., voltage requirements). This concern was evidenced in an analysis by the Australian Energy Market Operator, which showed that only a minority of the many examined inverters comply with the AS/NZS 4777.2 requirements [9].

Poor standard compliance levels can have significant implications, such as increased PV curtailment and reduced network stability limits [9]. Furthermore, the lack of knowledge of inverter control capabilities makes the results of optimal power flow [10] (or any "digital twin" functionality that aims to capture actual network behavior) untrustworthy, often precisely when it matters most, e.g., near the statutory limit of overvoltage. Incorrect assumptions on control settings could impact digital twins similarly to erroneous network models [11].

While it is unclear from public information how often IBR settings are changed in practice, the IEEE 1547-2018 standard mandates that IBRs have the ability to have their control settings "remotely programmed" by their "managing entities" [6]. As this feature becomes deployed in practice, grid operators will need to be aware of evolving control conditions across a portfolio of interconnected IBRs.

A. Related work

While extensive research has been performed on the data-driven estimation of network properties (impedances, connectivity, etc.), e.g., [12], [13], there is limited work on the identification of inverter control settings. Although increased telemetry in distribution networks facilitates system identification, PV systems are usually installed behind the meter (BTM) and utilities do not always have access to separate PV generation measurements, but only to net grid injection/demand. While this depends on the location and jurisdiction, if only net power measurements are available, disaggregation of the PV injection from the net load is necessary [14]. Furthermore, as these are privately owned assets, operators may lack knowledge of other PV system properties, e.g., their rating, tilt, and azimuth. Estimation of these properties can be beneficial for operators, e.g., to improve generation forecasts [15].

To the authors' knowledge (and as per the review in [11]), the only prior research paper on inverter control settings estimation is reference [16]. However, [16] assumes prior knowledge of the control law (i.e., constant power factor vs. volt-var), whereas even the latter is often unknown in practice.

B. Contributions

This paper fills this gap in the literature by developing methods to *classify* the type of reactive power control law that governs the behavior of a BTM inverter-based resource (IBR), particularly focusing on solar photovoltaic inverters. The candidate laws we consider are volt-var (vv) and fixed power factor (pf), the most common reactive power control modes. The data input to these classification methods are 15-minute-granularity advanced metering infrastructure (AMI) data, the most common data available to utilities [17].

We develop two methods: an intuitive method using the nearest centroid classifier and another method using a fully connected neural network (FCNN). Our numerical experiments with varying noise levels demonstrate both methods' performance. The results in this paper indicate that the neural network-based method achieves significantly higher accuracy.

The remainder of the paper is organized as follows. First, in Section II, we propose the two methods for classifying the control laws governing solar inverters based on smart meter data. In Section III, we present and analyze our results. In Section IV, we conclude the paper and provide future research directions.

II. Methodology

This section introduces two methods for addressing the reactive power control law classification problem. Relying on data-driven techniques, both methods require the availability of synthetic timeseries smart meter data associated with nodes where the governing control laws are correctly labeled as either volt-var, fixed power factor, or no solar inverter present. As we will discuss further in Section III-A, our numerical studies use data from a timeseries simulation of the 1379-node Ckt. 5 model in OpenDSS [18] with 701 solar PV inverters that have a mix of volt-var and fixed power factor control laws.

A. Nearest Centroid Classifier Method

At a conceptual level, our first proposed method is a clustering-style heuristic that classifies each recorded timeseries power injection profile according to its closeness to the mean profiles ("centroid") for each control law obtained from labeled timeseries data, after appropriate data normalization. This method relies on the assumption that nodes where the net injection is always negative (consistent net power consumption) do not have a solar generator present. While relatively simplistic, this method serves as a baseline for assessing the possible performance improvements that may be achieved via more sophisticated methods, such as our second method based on neural networks discussed later in this section.

The intuition for this clustering heuristic is based on the fact that the measurements obtained for the active and reactive power at a node are significantly impacted by the PV inverter's control law. More specifically, the reactive power output from a PV inverter is determined by the active power when set in fixed power factor control whereas the nodal voltage determines the reactive power output when volt-var control is employed. The relationships between the different quantities are given by the control laws' characteristic curves as discussed in [19], [20].

With this knowledge, we develop simulated, empirical sample estimates of the sample mean profiles for the active and reactive power injections associated with different control laws to estimate expected behaviors. Define $\mathcal{N} = \{1, \dots, N\}$ as the set of nodes for an N-bus system and $\mathcal{T} = \{1, \dots, T\}$ the set of T time periods. Let $P^*_{n,t}$ and $Q^*_{n,t}$ denote the measured values for active and reactive power injections at node $n \in \mathcal{N}$ and time $t \in \mathcal{T}$. To compute sample mean profiles that are meaningful across nodes with differing demands and solar PV inverter sizes, we first normalize the timeseries profiles of active and reactive power injection data, P^* and Q^*, by their maximum values to obtain normalized power injection profiles $P_{n,t}$ and $Q_{n,t}$:

$$P_{n,t} = \frac{P^*_{n,t}}{\max_{\tau \in \mathcal{T}} P^*_{n,\tau}},\ Q_{n,t} = \frac{Q^*_{n,t}}{\max_{\tau \in \mathcal{T}} Q^*_{n,\tau}},\ n \in \mathcal{N}, t \in \mathcal{T}.$$

Define the sets of nodes with volt-var and constant power factor control laws and no PV inverter present as $\mathcal{N}_{\mathsf{vv}}$, $\mathcal{N}_{\mathsf{pf}}$, and $\mathcal{N}_{\mathsf{no}}$, respectively. From the normalized data P and Q, we obtain the empirical average of the normalized active and reactive power injections, $\hat{P}$ and $\hat{Q}$, across nodes with a particular control law at each time $t \in \mathcal{T}$:

$$\begin{aligned}
\hat{P}_{\mathsf{vv},t} &= \frac{1}{|\mathcal{N}_{\mathsf{vv}}|} \sum_{n \in \mathcal{N}_{\mathsf{vv}}} P_{n,t}, & \hat{Q}_{\mathsf{vv},t} &= \frac{1}{|\mathcal{N}_{\mathsf{vv}}|} \sum_{n \in \mathcal{N}_{\mathsf{vv}}} Q_{n,t}, \\
\hat{P}_{\mathsf{pf},t} &= \frac{1}{|\mathcal{N}_{\mathsf{pf}}|} \sum_{n \in \mathcal{N}_{\mathsf{pf}}} P_{n,t}, & \hat{Q}_{\mathsf{pf},t} &= \frac{1}{|\mathcal{N}_{\mathsf{pf}}|} \sum_{n \in \mathcal{N}_{\mathsf{pf}}} Q_{n,t}, \\
\hat{P}_{\mathsf{no},t} &= \frac{1}{|\mathcal{N}_{\mathsf{no}}|} \sum_{n \in \mathcal{N}_{\mathsf{no}}} P_{n,t}, & \hat{Q}_{\mathsf{no},t} &= \frac{1}{|\mathcal{N}_{\mathsf{no}}|} \sum_{n \in \mathcal{N}_{\mathsf{no}}} Q_{n,t},
\end{aligned}$$

where $|\cdot|$ denotes the number of elements in a set. We thus have three sample mean profiles for active power, $\hat{P}_{\mathsf{pf}}$, $\hat{P}_{\mathsf{vv}}$, and $\hat{P}_{\mathsf{no}}$, and three sets for reactive power, $\hat{Q}_{\mathsf{pf}}$, $\hat{Q}_{\mathsf{vv}}$, and $\hat{Q}_{\mathsf{no}}$. A timeseries simulation of the Ckt. 5 model using OpenDSS [18] yields the sample mean curves shown in Fig. 1.

After establishing the mean profile for each of our three cases, we proceed with the classification. Given a timeseries of measured points $P^*_{n,t}$ and $Q^*_{n,t}$, $t \in \mathcal{T}$, from a smart meter at node n, the control law for the associated node is found by calculating the Euclidean norm between the normalized points and the sample mean profiles for the three different cases (vv, pf, and no). The input measurements are sampled over 24 hours at 15-minute granularity, although we note that any sufficiently long period could work. The *nearest centroid* for

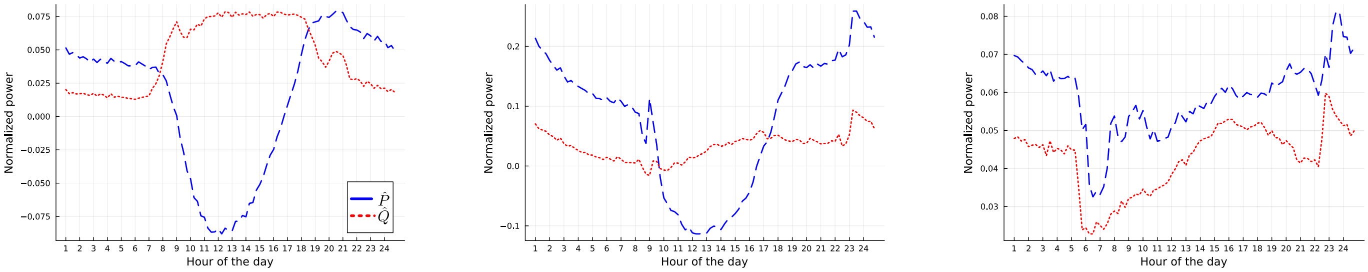

(a) Sample mean profile for volt-var control

(b) Sample mean profile for power factor control

(c) Sample mean profile for no control (no inverter present)

Fig. 1: Sample mean curve for the different control laws.

the solar PV inverter at node $n \in \mathcal{N}$ is obtained by determining which sample mean profile ($\hat{Q}_{\text{vv}}$ or $\hat{Q}_{\text{pf}}$) has smallest squared Euclidean distance in the reactive power injections across time:

$$\hat{h}_n = \underset{h \in \{\text{vv},\text{pf}\}}{\arg\min} \sum_{t \in \mathcal{T}} \left(Q_{n,t} - \hat{Q}_{h,t} \right)^2. \tag{1}$$

Only computing the distances for Q with respect to volt-var and power factor control is required in (1) because we perform a heuristic rejection step for nodes that never achieve a net positive active power injection, i.e., we assume that nodes where the net active power injections are always negative do not have solar PV inverters. This leads to the method shown in Algorithm 1.

Algorithm 1: Nearest Centroid Classifier

Input: P^*, Q^* ▷ Sets of measurement values
Output: Classifications for each node

Normalize: $P^* \rightarrow P, \quad Q^* \rightarrow Q$
foreach *node* $n \in \mathcal{N}$ **do**
  if $\min_{t \in \mathcal{T}}(P_{n,t}) \leq 0$ **then**
    if $\sum_{t \in \mathcal{T}} \left(Q_{n,t} - \hat{Q}_{\text{pf},t} \right)^2 \leq \sum_{t \in \mathcal{T}} \left(Q_{n,t} - \hat{Q}_{\text{vv},t} \right)^2$ **then**
      Classify node n as power factor controlled;
    else
      Classify node n as volt-var controlled;
  else
    Classify node n as no control (no inverter present);

B. Neural Network Based Method

The varying nature of smart meter measurements makes neural-network-based techniques viable candidates for classifying inverter control laws. In a supervised learning approach, we train a fully connected neural network (FCNN) that takes the timeseries of active and reactive power injections and voltage magnitudes at node $n \in \mathcal{N}$ as inputs to estimate a classification for the control law at this node.

The size of the input layer is an $n \times 3$ matrix, where n is the length of the time series measurement fed into the FCNN.

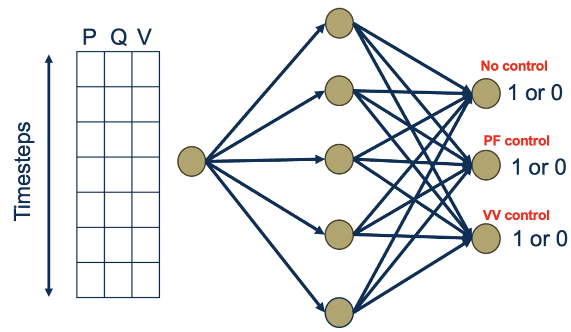

Fig. 2: The architecture of the fully connected neural network model for classifying a solar inverter's control law.

The output is a 3×1 vector representing the three possible classes. The output is modeled as a one-hot classifier, which produces *1* for the predicted/classified control law and *0* for the other outputs, as shown in Fig. 2. We design the FCNN to have two hidden layers, each with a `ReLU` activation function, while the output has the `softmax` activation function [21]. The number of neurons in the hidden layers is scaled by the size of the input matrix.

III. Numerical Results

In this section, we investigate how well the methods described in Section II perform the classification task and analyze the results obtained.

A. Setup and Dataset

To evaluate the performance of the methods, we utilized synthetic data obtained from the Ckt. 5 model of OpenDSS [18]. This dataset corresponds to a distribution network of 1379 nodes, 701 ($\approx 50\%$) of which have installed solar PV generators. The dataset includes solar panels with both power factor and volt-var control laws. The generated synthetic data consists of the P, Q, and V measurement values for all nodes and solar panels stemming from power flow calculations at 15-minute intervals. The control laws are correctly labeled for each solar panel, enabling them to be used for all experiments. The labels are distributed as follows: 32.70% nodes with volt-var control, 18.13% nodes with power factor control, and 49.17% nodes with no PV.

The main metric for assessing performance in our results section is prediction accuracy, which is defined as the percentage of nodes for which the control law is correctly classified:

$$\text{accuracy} = \frac{1}{|\mathcal{N}|}\sum_{n\in\mathcal{N}} \mathbb{1}\{\hat{y}_n = y_n\} \times 100 \quad [\%], \tag{2}$$

where $\hat{y}_i$ is the predicted label, y_i is the true label, and $\mathbb{1}\{\hat{y}_i = y_i\}$ is the indicator function (1 if $\hat{y}_i = y_i$ and 0 otherwise).

B. Nearest Centroid Classifier Results

We classify the measurements into three control laws using the algorithm detailed in Algorithm 1. Out of the 1379 nodes in our dataset, we generate our sample mean profiles using 1100 nodes ($\approx 80\%$) and test on the remaining 279 nodes. We refer to these as our training and testing datasets, respectively. For the training dataset, we utilize all the data points to generate the sample mean daily profiles for the active and reactive power. The testing is done by applying Algorithm 1 to day-long samples for each node in the test dataset, i.e., 96 samples each day.

Due to the seasonal differences in the load profile and changes in solar radiation, we present the results on a month-by-month basis vs. a year-long basis to observe the difference. We do this to investigate the effect of seasonally dependent curves versus implementing a year-long analysis (seasonal effects ignored). The results are given in Table I.

The results show that using a year-long estimate performs better on average, despite some months having higher prediction accuracies than the year-long dataset.

C. Neural Network-Based Classification Results

The flexibility of neural networks allows for variation in the structure of the inputs. This subsection focuses on experiments to find the FCNN structure in terms of the timeseries length that gives the most accurate results.

Smart meter measurements come in abundance for different electrical quantities. This raises the question of how many data points are "enough" to predict the control laws correctly. To answer this, we trained different FCNNs that receive varying numbers of inputs for differing amounts of timeseries data and applied these neural networks to classify the testing dataset.

TABLE I: Prediction accuracy of Nearest Centroid classifier

Month	Prediction Accuracy (%)
January	86.18
February	86.37
March	86.68
April	85.17
May	82.99
June	69.73
July	66.73
August	66.83
September	70.91
October	84.62
November	83.49
December	81.50
Monthly Average	**79.27**
Yearly	**83.22**

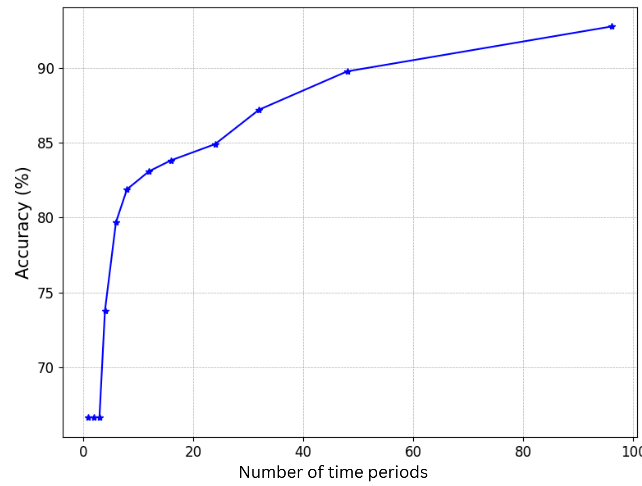

Fig. 3: Impact of the number of input time periods on the neural network's classification accuracy.

This allows us to assess how the number of time periods affects the performance of the neural network classifier. The fully connected neural network was built and trained using TensorFlow [22] with the AdaMax Optimizer. For uniformity, the batch size was set to 128, with a dropout of 0.25 and a maximum number of epochs capped at 50 for all experiments. Similar to Section III-B, the first 1100 nodes are used to train neural networks, while the rest are reserved as testing datasets.

Fig. 3 shows that the accuracy of the neural network-based classification increases with the length of the input time series, which is expected. The steeper increases in accuracy occur between eight and twenty-four time periods, and limited gains are registered after forty-eight time periods (i.e., 12 hours). Using the entire day yields a maximum accuracy of 92.75%. Analyzing the effects of seasonal variation on our neural network classifier will be investigated in our future work.

D. Comparing Methods

Finally, we present a detailed comparison of the two methods to assess their performance. We analyze the methods' ability to accurately classify the control law used in a particular inverter, given the set of smart meter measurements under the same conditions. We add noise to the measurement to emulate real-world conditions and assess how such measurement errors affect the two methods.

As is conventional in the literature, measurement errors are assumed to be independent and normally distributed, with a standard deviation equal to one-third of the maximum error [23]. The value of the measured quantity with error is usually represented as

$$X \sim \mathcal{N}\left(X^\dagger, \frac{0.005 \times X^\dagger}{3}\right), \tag{3}$$

where $X^\dagger$ is the actual value of the quantity and the maximum error is 0.5% of the true value ($0.005 \times X^\dagger$). Using this for-

		Predicted scheme		
		NO	PF	VV
Actual scheme	NO	51.97%	0.00%	0.00%
	PF	0.77%	3.12%	12.60%
	VV	1.20%	2.22%	28.13%

(a) Centroid-based classifier

		Predicted scheme		
		NO	PF	VV
Actual scheme	NO	49.08%	0.02%	0.08%
	PF	0.21%	12.31%	5.71%
	VV	0.42%	4.85%	27.33%

(b) Neural network classifier

TABLE II: Confusion matrices for the two classification models. Diagonal entries represent correct predictions as a percentage of the total predictions.

mulation for randomized error, we compare the two methods and their ability to make accurate predictions.

The accuracy of the centroid classifier is 82.79%. In contrast, the neural network classifier has a classification accuracy of 92.52%, i.e., a 10% accuracy advantage.

For further analysis, we investigate the estimates in more detail. Tables II(a) and II(b) are two confusion matrices showing the percentage of true positives and false negatives in the predictions for the different methods.

For the centroid-based classifier results in Table IIa, we observe a perfect prediction, with no false positives, for nodes without PV inverters. This classifier tends to make more false positive predictions of the volt-var control law, indicating a bias towards this prediction. On the other hand, in addition to being more accurate, the neural network classifier results in Table IIb show a relatively more uniform distribution of false predictions for the different control laws. Unlike the centroid classifier, the neural network method had no clear propensity towards any of the control laws.

Another metric for studying the performance of these methods is their receiver operating characteristic curve, which describes the classifier's performance under varying threshold levels [24]. This is only relevant to the neural network classifier. Fig. 4 shows the receiver operating characteristics curve. The area under the curve (AUC) values are all near one, indicating good classification performance.

Finally, we illustrate the robustness of the different methods to varying levels of measurement noise. In (3), we model the maximum error possible as 0.5% of the actual value. To assess the performance of these methods in the presence of varying noise, Fig. 5 shows the classifier accuracy with maximum errors ranging from 0% to 5%.

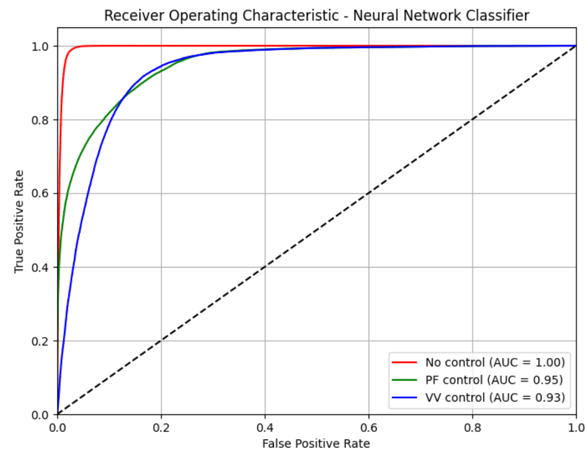

Fig. 4: Receiver operating characteristic curve for the neural network classifier.

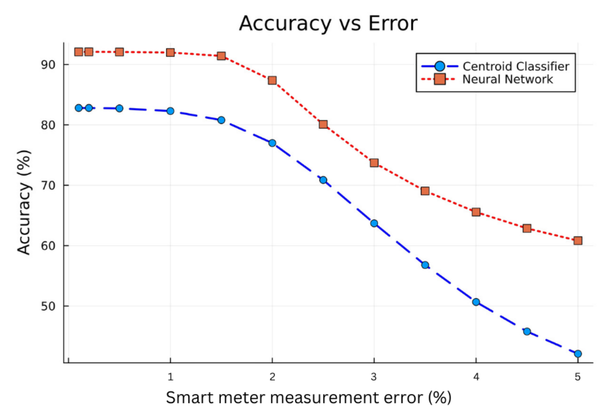

Fig. 5: Variation of classification accuracy vs. smart meter measurement error.

The figure shows that the neural network consistently outperforms the centroid classifier. Interestingly, while the accuracies of both methods decrease with increasing measurement noise, the rate of decline of the centroid classifier is steeper, particularly in considerably noisy scenarios ($\geq 3\%$).

IV. Conclusion

As distribution utilities face increasing installations of inverter-based resources, identifying their control laws, which are usually unknown, is essential for network safety and efficient management.

This paper presents two data-driven methods to classify reactive power control laws of solar PV inverters in distribution networks from smart meter measurements. The first method is based on a nearest centroid approach and the second on a neural network. The results show that the methods can accurately classify nodes as having an inverter with constant power factor control, an inverter with volt-var control, or the absence of an inverter. We compare the two methods, showing their performance under varying levels of measurement noise, and investigating their biases towards any of the control laws. Our neural network-based method performs well even with increasing levels of measurement noise and shows no biases towards any of the control laws.

A primary limitation of the work conducted to date is that we have only considered volt-var and fixed power factor control laws. Several other control paradigms, such as volt-watt control and frequency droop control, could be considered in future work.

Furthermore, as this is, to our knowledge, the first paper to address the problem of inverter control law identification, we deem it of interest to develop and test additional methods. A simple potential improvement, for instance, could combine the two methods: using the nearest centroid classifier to detect the nodes with no PV with high accuracy, and then applying a neural network classifier to the remaining datasets.

ACKNOWLEDGMENT

The authors thank Joseph Azzolini for his early assistance with the OpenDSS simulation pipeline and Jaimie Swartz for her insightful comments on an early version of this manuscript.

REFERENCES

[1] K. Baker, A. Bernstein, C. Zhao, and E. Dall'Anese, "Network-cognizant design of decentralized Volt/VAR controllers," in *IEEE Power Energy Society Innovative Smart Grid Technologies Conf*, pp. 1–5, Apr. 2017.

[2] M. Zholbaryssov and A. D. Domínguez-García, "Safe Data-Driven Secondary Control of Distributed Energy Resources," *IEEE Trans. Power Syst.*, vol. 36, pp. 5933–5943, Nov. 2021.

[3] X. Zhou, et al., "Reverse and Forward Engineering of Local Voltage Control in Distribution Networks," *IEEE Trans. Autom. Control*, vol. 66, pp. 1116–1128, Mar. 2021.

[4] J. Swartz and A. Von Meier, "The Impact of Three-phase Impedances on the Stability of DER Systems," in *North American Power Symposium*, pp. 1–6, 2021.

[5] J. Swartz, F. Celi, F. Pasqualetti, and A. Von Meier, "Parameter Conditions to Prevent Voltage Oscillations Caused by LTC-Inverter Hunting on Power Distribution Grids," in *European Control Conference*, pp. 1118–1125, 2022.

[6] "IEEE Standard for Interconnection and Interoperability of Distributed Energy Resources with Associated Electric Power Systems Interfaces," *IEEE Std 1547-2018 (Revision of IEEE Std 1547-2003)*, pp. 1–138, Apr. 2018.

[7] Hawaiian Electric Company, Inc, "Rule No. 14, ," *Service connections and facilities on customer's premises, Hawaiian Electric*, 2021.

[8] "Grid Connection of Energy Systems via Inverters, Part 2: Inverter Requirements," *AS/NZS 4777.2:2020*, 2020.

[9] Australian Energy Market Operator, "Compliance of Distributed Energy Resources with Technical Settings. Compliance to AS/NZS4777.2; A technical report for Australia," pp. 1–75, 2023.

[10] A. Inaolaji, A. Savasci, and S. Paudyal, "Distribution Grid Optimal Power Flow in Unbalanced Multiphase Networks With Volt-VAr and Volt-Watt Droop Settings of Smart Inverters," *IEEE Trans. Ind. Appl.*, vol. 58, no. 5, pp. 5832–5843, 2022.

[11] F. Geth, M. Vanin, W. Van Westering, T. Milford, and A. Pandey, "Making Distribution State Estimation Practical: Challenges and Opportunities," *arXiv:2311.07021*, 2023.

[12] V. C. Cunha et al., "Automated Determination of Topology and Line Parameters in Low Voltage Systems Using Smart Meters Measurements," *IEEE Trans. Smart Grid*, vol. 11, no. 6, pp. 5028–5038, 2020.

[13] M. Vanin, F. Geth, R. D'hulst, and D. Van Hertem, "Combined Unbalanced Distribution System State and Line Impedance Matrix Estimation," *Int. J. Elect. Power Energy Syst.*, vol. 151, p. 109155, 2023.

[14] C. C. Liu, H. Chen, J. Shi, and L. Chen, "Self-supervised Learning method for Consumer-level behind-the-meter PV estimation," *Applied Energy*, vol. 326, p. 119961, 2022.

[15] K. Mason, M. J. Reno, L. Blakely, S. Vejdan, and S. Grijalva, "A Deep Neural Network Approach for Behind-the-meter Residential PV size, tilt and azimuth estimation," *Solar Energy*, vol. 196, pp. 260–269, 2020.

[16] S. Talkington, S. Grijalva, M. J. Reno, and J. A. Azzolini, "Solar PV Inverter Reactive Power Disaggregation and Control Setting Estimation," *IEEE Trans. Power Syst.*, vol. 37, no. 6, pp. 4773–4784, 2022.

[17] J. Peppanen, M. Hernandez, J. Deboever, M. Rylander, and M. J. Reno, "Distribution Load Modeling – Survey of the Industry State, Current Practices and Future Needs," in *53rd North American Power Symposium*, Nov. 2021.

[18] R. C. Dugan and T. E. McDermott, "An Open Source Platform for Collaborating on Smart Grid Research," in *IEEE Power and Energy Society General Meeting*, 2011.

[19] M. Jafari, T. Olowu, and A. Sarwat, "Optimal Smart Inverters Volt-VAR Curve Selection with a Multi-Objective Volt-VAR Optimization using Evolutionary Algorithm Approach," *IEEE Trans. Smart Grid*, 2025.

[20] R. Heidari and F. Geth, "Improved Algebraic Inverter Modeling for Four-Wire Power Flow Optimization," *Electric Power Systems Research*, vol. 234, p. 110825, 2024. presented at *23rd Power Systems Computation Conference (PSCC)*.

[21] J. S. Bridle, "Probabilistic Interpretation of Feedforward Classification Network Outputs, with Relationships to Statistical Pattern Recognition," in *Neurocomputing: Algorithms, Architectures and Applications*, pp. 227–236, Springer, 1990.

[22] M. Abadi, et al., "TensorFlow: Large-Scale Machine Learning on Heterogeneous Distributed Systems," *arXiv:1603.04467*, 2016.

[23] M. Deakin, M. Vanin, Z. Fan, and D. Van Hertem, "Smart Energy Network Digital Twins: Findings from a UK-based Demonstrator Project," *Int. J. Elect. Power Energy Syst.*, vol. 162, p. 110302, 2024.

[24] T. Fawcett, "An Introduction to ROC Analysis," *Pattern Recognition Letters*, vol. 27, no. 8, pp. 861–874, 2006.